Visualizing the effects of Lactate Dehydrogenase (LDH) inhibition and *LDH-A* genetic ablation in breast and lung cancer with hyperpolarized pyruvate NMR

Gopal Varma[1,#], **Pankaj Seth**[2,#], **Patricia Coutinho de Souza**[1], **Cody Callahan**[1], **Jocelin Pinto**[3], **Manushka Vaidya**[1,3], **Olmo Sonzogni**[3], **Vikas Sukhatme**[2,4], **Gerburg M. Wulf**[3], **Aaron K. Grant**[1,*]

[1]Department of Radiology, Beth Israel Deaconess Medical Center, Harvard Medical School, Boston, MA 02215, USA

[2]Department of Medicine, Beth Israel Deaconess Medical Center, Harvard Medical School, Boston, MA 02215, USA

[3]Department of Hematology and Oncology, Beth Israel Deaconess Medical Center, Harvard Medical School, Boston, MA 02215, USA

[4]Department of Medicine, Emory University School of Medicine, Atlanta, GA 30322, USA

Abstract

In many tumors, cancer cells take up large quantities of glucose and metabolize it into lactate, even in the presence of sufficient oxygen to support oxidative metabolism. It has been hypothesized that this malignant metabolic phenotype supports cancer growth and metastasis, and that reversal of this so-called 'Warburg effect' may selectively harm cancer cells. Conversion of glucose to lactate can be reduced by ablation or inhibition of lactate dehydrogenase (LDH), the enzyme responsible for conversion of pyruvate to lactate at the endpoint of glycolysis. Recently developed inhibitors of lactate dehydrogenase provide new opportunities to investigate the role of this metabolic pathway in cancer.

Here we show that magnetic resonance spectroscopic imaging (MRSI) of hyperpolarized pyruvate and its metabolites in models of breast and lung cancer revealed that inhibition of LDH was readily visualized through reduction in label exchange between pyruvate and lactate, while genetic ablation of the *LDH-A* isoform alone had smaller effects. During the acute phase of LDH inhibition in breast cancer, no discernible bicarbonate signal was observed and small signals from alanine were unchanged.

Graphical Abstract

[*] **Corresponding author:** Aaron K. Grant, PhD, Department of Radiology, Division of MR Research, Beth Israel Deaconess Medical Center, Harvard Medical School, AN-232, 330 Brookline Avenue, Boston, MA 02215, USA, akgrant@bidmc.harvard.edu.
[#]GV and PS contributed equally to this work

• Hyperpolarized ^{13}C pyruvate magnetic resonance spectroscopic imaging (MRSI) was used to investigate the metabolic pathway following LDH inhibition in models of breast and lung cancer, as well as *LDH-A* genetic ablation in the latter.

• A consistent reduction in label exchange between hyperpolarized pyruvate and lactate was visualized by MRSI following LDH inhibition by the drug GNE-140.

• Tamoxifen-induced deletion of the *LDH-A* isoform alone showed a small, non-significant reduction in hyperpolarized pyruvate to lactate exchange.
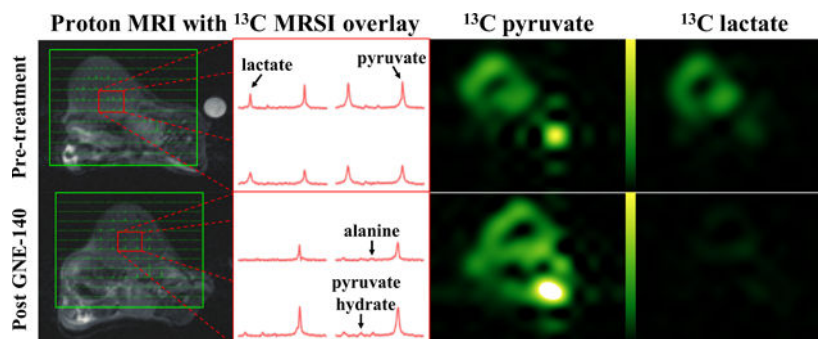
Keywords

Cancer metabolism; GNE140; hyperpolarized ^{13}C pyruvate; LDH; LDH-A; MRSI; Warburg effect

Introduction

Metabolic reprogramming in cancer manifests differently depending upon specific oncogenic drivers. However increased uptake of glucose, coupled with preferential conversion of glucose to lactate, is a generic feature shared broadly across many types of cancer. While the precise role of this metabolic phenotype, known as the Warburg effect[1], is not fully understood, it has been hypothesized that conversion of glucose to lactate supports cancer growth and metastasis by reducing oxidative stress on cancer cells[2,3], enabling cells to adapt to a hypoxic tumor microenvironment[4], suppressing immune responses[5,6], and providing trioses for anabolic processes[7,8]. The Warburg effect therefore presents a target for therapy, to the extent that inhibition of enzymes involved in glycolytic fermentation can deprive cancer cells of their preferred source of energy and trioses. Within this framework, lactate dehydrogenase (LDH), the enzyme that converts pyruvate to lactate at the endpoint of glycolysis, is a promising target. Inhibition of LDH blocks a key metabolic step of the Warburg physiology while preserving the upstream glycolytic chain, disrupting the regeneration of NAD+ necessary for continued glycolytic flux and potentially increasing the more efficient ATP generation via the TCA cycle. This in turn may inhibit tumor growth and metastasis by increasing oxidative stress[2,3], depriving cancer cells of the ability to survive in a hypoxic tumor microenvironment[4], and reducing extracellular acidification by lactate[9].

LDH is a tetrameric enzyme consisting of four subunits encoded by the genes *LDH-A, LDH-B*, and the testes-specific *LDH-C*. Although each catalyzes a rapid exchange of pyruvate and lactate, the A and B isoforms of LDH have different substrate affinities, with

LDH-A preferentially converting pyruvate to lactate and LDH-B preferentially mediating the reverse reaction. In many cancers, oncogenic signaling drives overexpression of hypoxia-inducible factor 1α (HIF1α), which in turn drives increased levels of LDH-A. It has been hypothesized that ablation of LDH-A may have therapeutic value in tumors as it limits the Warburg effect by shuttling pyruvate away from lactate to the TCA cycle. It has been demonstrated that *LDH-A* suppression in cultured cancer cells enhances the Krebs cycle and oxygen consumption, resulting in increased production of reactive oxygen species and apoptosis in cancer cells[10,11].

In this work, hyperpolarized magnetic resonance spectroscopic imaging (MRSI) of [1-^{13}C]pyruvate and its metabolites was employed as a tool to non-invasively investigate the effects of lactate dehydrogenase inhibition in models of breast and lung cancer. It should be noted that the lactate signal observed with hyperpolarized pyruvate has a complex dependence on many factors in addition to LDH activity, including monocarboxylate transporter (MCT) activity, the lactate pool size, and tissue redox balance[12,13]. Nevertheless, many studies have shown that the lactate signal in cancer is modulated (and generally reduced) in response to a range of chemotherapeutic interventions[12,14–16]. The role of LDH specifically has been investigated using the candidate inhibitor FX-11, with the conclusion that this compound leads to a gradual, roughly 40% reduction in lactate signal over a period of several days in a xenograft model of lymphoma[17]. A recently developed inhibitor of LDH, GNE140[18], has presented new opportunities to examine the role of LDH inhibition to treat cancer and to investigate the ability of non-invasive imaging to interrogate the effects of candidate inhibitors. Effects of the inhibitor GNE140 have been investigated using a variety of assays including ^{18}FDG-PET in pancreatic cancer cell lines and *ex vivo* analysis of metabolites in tissue excised from pancreatic cancer xenografts. These studies showed that GNE140 reduced FDG uptake in cell culture, increased production of reactive oxygen species, and reduced lactate formation in xenografts[18]. However, the therapeutic benefit to block the growth of tumors *in vivo* was limited, and it was suggested that the inherent metabolic plasticity of tumor cells requires a collaborative approach such as combining an LDH inhibitor with compounds targeting oxidative phosphorylation or the AMPK-S6K signaling axis[18].

The present work demonstrates that hyperpolarized pyruvate enables non-invasive visualization of acute LDH inhibition within 30 minutes of treatment, with a roughly 80% reduction in lactate signal observed in syngeneic, immune competent models of breast and lung cancer. In a tamoxifen-inducible *LDH-A* genetic knockout model of lung cancer however, the effects of selective *LDH-A* deletion on pyruvate to lactate interconversion were comparatively modest, suggesting that combined extinction of *LDH-A* and *LDH-B* is required for effective shutdown of lactate production in tumors, in concordance with recent studies of double genetic ablation of *LDH-A* and *LDH-B*[19].

Experimental

Cancer Models and Modulation of LDH Activity—Animal studies were undertaken with the approval of the local Institutional Animal Care and Use Committee. We tested the acute pharmacodynamics of LDH inhibition in two different models of common

epithelial malignancies, triple-negative breast cancer (TNBC), and non-small cell lung cancer (NSCLC). TNBC was induced using Cre-mediated knock-out of *BRCA1* and *p53*[20]. Primary tumors were banked and propagated using syngeneic transplantation as described previously[14,21]. In these models we had previously shown that tumors exhibit high glucose avidity as indicated by ^{18}F-fluorodeoxyglucose PET as well as a high degree of pyruvate-to-lactate interconversion indicative of a high degree of LDH activity[14]. Tumors in the TNBC model were allowed to grow to a size of approximately 10±5mm (along their longest axis) prior to imaging. A model of NSCLC was employed to address the contribution of the *LDH-A* isoform to total LDH activity *in vivo*. Briefly, *Cre[tm]-LDH-A^{fl/fl};Ccsp-rtTA/(tetO)-EGFR-L858R-T790M* mice were generated[10] using our own conditional *LDH-A*-knockout mice crossbred with a NSCLC model of EGFR activation[22], and tumors were induced in lung tissue by mutant *EGFR-L858R-T790M* with doxycycline diet (625ppm in standard chow). This model has been described previously[10], and the reduction in LDH-A following tamoxifen administration has been demonstrated by Western blot analysis[10]. Tumors were allowed to grow until solid masses were apparent on MR images of the lungs before undertaking imaging with hyperpolarized pyruvate as described below.

For studies making use of GNE140, animals underwent hyperpolarized imaging twice during the same session. Approximately 10 minutes after the first hyperpolarized acquisition, animals received 100mg/kg GNE140 dissolved in DMSO via intra-peritoneal injection. Thirty minutes later, hyperpolarized imaging was repeated. For studies making use of the *Cre[tm]-LDH-A^{fl/fl};Ccsp-rtTA/(tetO)-EGFR-L858R-T790M* model, animals underwent hyperpolarized imaging in two sessions separated by 7 days. Starting immediately after the first imaging session, *LDH-A* deletion was initiated by administration of tamoxifen IP, 100mg/kg, for three consecutive days.

Animal Handling—Prior to imaging, mice were anesthetized with isoflurane in oxygen administered via nose cone. A 30G needle connected to an extension tube was placed in the tail vein, and the animal was then placed at scanner isocenter with respiratory and temperature monitoring. A feedback-controlled warm air circulator maintained the superficial body temperature, measured by an optical probe place on the animal's abdomen, at 36°C.

Preparation of Hyperpolarized Pyruvate—Hyperpolarized pyruvate solution was prepared by dynamic nuclear polarization (DNP) using a commercial DNP polarizer (Hypersense, Oxford Instruments Molecular Biotools, Oxfordshire UK). [1-^{13}C]pyruvic acid was combined with 15mM OX063 radical (GE Healthcare, London UK) and 1mM gadoteridol (ProHance, Bracco, Milan Italy) and polarized for 40 minutes or more at 1.4K and 100mW microwave power. The polarized material was then dissolved in saline containing 50mM TRIS and 125mg/l EDTA and adjusted to physiological pH with sodium hydroxide to obtain 96mM hyperpolarized pyruvate solution for injection. 250μl of this solution were administered as a 10–15s intravenous bolus starting a few seconds after the initiation of the ^{13}C MRSI acquisition.

Hyperpolarized Magnetic Resonance Imaging—Imaging studies were conducted using a 9.4T horizontal bore magnet (Bruker Biospec, Billerica MA). [13]C and proton images

were acquired with either: an 84mm quadrature proton coil and an in-house built 27mm transmit/receive ^{13}C surface coil; or, a 72mm dual-tuned ^{1}H/^{13}C volume coil and a 27mm ^{13}C receive-only surface coil (Rapid MR, Rimpar Germany). Breast cancer studies and *LDH-A* deletion studies in the lung made use of the transmit/receive surface coil. Lung studies with GNE140 made use of the receive-only surface coil. The choice was dictated by coil availability at the time of each series of scans.

Imaging protocol—Proton anatomic images were acquired using fast spin-echo sequences to confirm the position of the tumor and to provide an anatomic reference for ^{13}C spectroscopic images. For breast tumors a point-resolved spectroscopy (PRESS) sequence was used to perform local shimming within the tumor. ^{13}C images were acquired using echo-planar spectroscopic imaging (EPSI) with 4° tip angle, 16×16 matrix, 2.5mm in-plane resolution, approximately 5mm slice thickness, 512 spectral points, and 4kHz spectral width. 32 repetitions were acquired with 2s temporal resolution. EPSI acquisition was initiated immediately prior to the start of the pyruvate injection. Subcutaneous breast tumors were imaged using an axial slice, while lung tumors were imaged with a coronal slice whose position and thickness were adjusted to exclude the heart and large blood vessels to the extent possible. Respiratory gating was employed in lung studies to reduce motion artifacts. Thus, image acquisition was briefly halted during a narrow window around each inspiration/ expiration cycle. Owing to the intermittent character of the mouse respiratory waveform, it was possible to obtain a roughly 90% duty cycle with gated imaging.

Image reconstruction and analysis—Spectroscopic image data were separated into even and odd echoes, apodized with a 30Hz line-broadening filter, and reconstructed with standard Fourier methods to obtain pixel-by-pixel spectra with 2kHz spectral width. Spectra from even and odd echoes were then combined after application of a first-order phase to account for the temporal offset between the starting points of the two echo trains. Pixel-by-pixel magnitude spectra were computed, and metabolite signals were quantified by integrating their spectral peaks, after subtracting the mean magnitude noise from the spectra to eliminate spurious baseline signals. Magnitude noise was estimated from a noise-only spectrum. Metabolite images were resized to 128-by-128 matrices by zero fill interpolation and matched to the anatomical proton images. Regions of interest (ROIs) covering the tumors were drawn on the anatomical proton images, and metabolite signals were obtained from the sum of the pixel intensities over the ROIs in the resized ^{13}C images. Lactate-to-pyruvate ratios were computed using the time integrals of each metabolite's signal, a measure that has been shown to reflect the rate of label exchange between pyruvate and lactate[23].

Immunohistochemical Staining and Correlation with Image Data—To assess levels of LDH-A, MCT1, and MCT4 proteins in the *Cre^{tm}-LDH-A$^{fl/fl}$;Ccsp-rtTA/(tetO)-EGFR-L858R-T790M* model after administration of tamoxifen, immunohistochemical (IHC) staining of paraffin-embedded lung tissue was performed in a subset of the animals that exhibited localized lung masses. Additional samples from animals with intact *LDH-A* were also analyzed. IHC for LDH-A was conducted following standard IHC procedures including heat-based antigen retrieval in a citrate-buffer[24] and using a LDH-A-antibody

(Thermo Fisher PA5–79593). Staining for MCT1 and MCT4 employed the same methods and made use of antibodies PA5–72957 and PA5–8000 respectively (Invitrogen). MCT staining was performed in animals that had received tamoxifen and in untreated animals. Because LDH-A levels were found to vary widely between different lesions, tissue samples were subjected to Aperio scanning (Leica Biosystems), and LDH-A levels quantified by computing the percentage of pixels within each mass that showed positive staining for LDH-A. For those lesions that could be clearly correlated with masses seen on ^{1}H and ^{13}C images, metabolite ratios were computed using ROI methods as described above.

Statistical Analysis—Metabolite signals before and after LDH inhibition or ablation were compared using a paired two-tailed *t*-test. The linear association between results for immunoexpression of LDH-A and lactate-to-pyruvate ratios were calculated using the square of the Pearson product-moment correlation coefficient, R^2.

Results

Inhibition of LDH with GNE140

Administration of the drug GNE140 showed a consistent reduction in lactate-to-pyruvate ratios in the tumors from a model of BRCA1-related breast cancer, in which we have previously shown high glucose avidity and detectable pyruvate to lactate interconversion[14,21,24]. As expected, representative images and spectra demonstrate a visible lactate signal and sizeable lactate peaks prior to GNE140 administration (Fig. 1a). 30±5 minutes after treatment with GNE140, a negligible lactate signal was observed with lactate peaks (if any) comparable to peaks from alanine (Fig. 1b). No significant change was measured between alanine-to-pyruvate ratios pre- and post-treatment (Fig. 1c). Lactate signal in mice that received GNE140 showed an approximately 80% reduction, with significance *p*<0.001 (Fig. 1d). In control animals that received the vehicle DMSO only, the lactate signal was largely unchanged, showing a modest, non-significant increase. The spectra showed no discernible bicarbonate signal before or after treatment with GNE140 (Figs. 1a-b), measurement of which was confounded further by the bicarbonate peak being aliased to a position near lactate because of the 2kHz spectral width of the EPSI acquisition.

Similar results were observed in the *Ccsp-rtTA/(tetO)-EGFR-L858R-T790M* model of NSCLC. Lactate-to-pyruvate ratios showed a marked reduction following administration of GNE140. Despite the challenges of MRSI in the lung, respiratory gating allowed us to obtain measurable peaks from the metabolites associated with injection of [1-^{13}C]pyruvate from the MRSI data (Fig. 2). In the three treated animals, the lactate-to-pyruvate ratios fell to roughly 10% of their pre-treatment values. In three control animals injected with DMSO, the lactate-to-pyruvate ratio increased by 17–46%. Again, similar to the breast cancer model, no appreciable bicarbonate signal was apparent either before or after treatment. Scatter plots of the pre- and post-treatment lactate-to-pyruvate ratios are shown in Figure 2c.

Deletion of LDH-A in lung cancer

In a *Cre^{tm}-LDH-A$^{fl/fl}$;Ccsp-rtTA/(tetO)-EGFR-L858R-T790M* model with tamoxifen-inducible deletion of *LDH-A*, multiple spontaneous lung tumors emerged in animals

following induction of mutant *EGFR* by doxycycline chow. Consistent with the expected glycolytic phenotype of this model, a strong lactate signal was observed in the lung tumors. Spectra and images from ^{13}C MRSI showed that strong lactate signal was present in lung masses both pre- and post- deletion of *LDH-A* (Fig. 3). Signal from pyruvate was high both within lung masses as well as the large vessels, reflecting the presence of intravascular pyruvate following intravenous injection. In contrast to acute pharmacological inhibition with GNE140, mean lactate-to-pyruvate ratios (n=8) pre- and post-treatment with tamoxifen demonstrated a small reduction, from 0.46±0.25 to 0.44±0.20 (mean ± standard deviation), that was not considered significant (p=0.197, Fig. 3c). In a single additional animal, lung masses seen in the pre-deletion images were largely absent one week later. Although this animal did show a modest increase in lactate signal, it was excluded from this analysis because of the lack of apparent tumor tissue in the post-deletion study.

Immunohistochemical analysis of LDH-A and MCT1,4

To obtain further insight into the relationship between LDH-A protein levels and pyruvate-to-lactate interconversion by hyperpolarized MRSI, IHC staining was performed on tissue taken from a subset of the *Cre^{tm}-LDH-A$^{fl/fl}$;Ccsp-rtTA/(tetO)-EGFR-L858R-T790M* animals that underwent ^{13}C imaging as described in the preceding paragraph. Staining of tissues from a separate cohort of animals with intact *LDH-A* was also performed for comparison. We observed that, while there was wide variability between lesions with regard to LDH-A protein expression, within discrete solid masses the level of LDH-A protein was relatively constant. From 3 of the 8 animals analyzed that underwent tamoxifen-induced *LDH-A* deletion and ^{13}C imaging, 10 discrete lesions were identified on IHC-stained tissue slices. The fraction of LDH-A positive pixels for each lesion was then computed. The average fraction of positive pixels for the 10 lesions was (30±21)% (mean±standard deviation, range of 9 to 70%). By comparison, in 6 animals with intact *LDH-A*, the average over 30 discrete lesions was (85±16)%, ranging from 30 to 98%. To assess for correlation between LDH-A protein levels and imaging-based lactate-to-pyruvate ratios on a lesion-by-lesion basis, the IHC slices and ^{1}H images were inspected to identify all lesions that were common between the IHC and ^{13}C data. Seven such lesions were identified. The percentage of LDH-A IHC-positive pixels was then plotted against the lactate-to-pyruvate ratios computed from ROIs placed over the same lesions in the ^{13}C images (Fig. 4). The lactate-to-pyruvate ratio showed only a loose correlation with levels of LDH-A in tissue, with a correlation coefficient R^2=0.11.

Expression of MCT1 and MCT4 was assessed by IHC staining of tissue samples from the same cohort of three animals that had undergone *LDH-A* IHC analysis and in a second cohort of animals with intact *LDH-A*. The antibody stained robustly positive in the adjacent musculature as well as in mononuclear cells which served as an internal control (Fig. 5). In lung tumor tissues of mice whose tumors were induced by mutant EGFR, expression of these transporters was heterogenous, but consistently lower than in the adjacent muscle. Staining patterns were similar in EGFR-mutant tumors with or without ablation of *LDH-A*. These data suggest there is no dramatic upregulation of MCT1 or MCT4 upon LDH-A ablation in these tumors.

Limitations of the current study and directions for future work

A number of limitations of the current study should be noted. First, while the effects of *LDH-A* suppression on metabolic flux in cell culture were studied in[10,11], the current study lacks an LDH activity assay in the *Cre[tm]-LDH-A^{fl/fl};Ccsp-rtTA/(tetO)-EGFR-L858R-T790M* model. The reduction of *LDH-A* following tamoxifen treatment in this specific model, *Cre[tm]-LDH-A^{fl/fl};Ccsp-rtTA/(tetO)-EGFR-L858R-T790M*, has previously been confirmed by Western blot[10]. Confirmatory IHC staining for LDH-A in the specific tissue samples in our study was possible only in a subset of the animals owing to technical difficulties in the sample preparation that resulted in high levels of artifactual non-specific staining in the remaining cases.

The lactate pool is an important determinant of the lactate/pyruvate ratios observed using hyperpolarized ^{13}C, and ^1H MRS of lactate could shed further light on the observations presented here. The coils employed in the current study were optimized for ^{13}C sensitivity. Performing simultaneous ^1H spectroscopy would have been prohibitively complex, requiring multiple hardware changes during a single study. However, the question of the lactate pool size remains an interesting and important question for future studies. Further insights into altered metabolic flux during LDH inhibition could be addressed by cell culture studies using metabolic analyzers such as the Seahorse (Agilent Technologies, Santa Clara CA).

Additionally, future studies would benefit from an assessment of the toxicity profile of GNE140 administered IP.

Discussion

LDH inhibitors were developed with the expectation that disruption of the Warburg effect might substantially reduce the growth of tumor cells with high glycolytic activity. However it turned out that tumors exhibited primary, as well as secondary, adaptive resistance to LDH inhibition, mediated by activation of AMPK and upregulation of oxidative phosphorylation *in vitro*, explaining why GNE140 in mouse xenografts only delayed tumor growth, rather than cause tumor shrinkage when administered as a single agent[18]. The activity of GNE140 is further hampered by its relatively short (~6 hours) period of *in vivo* activity. Studies with hyperpolarized pyruvate at different time points following GNE140 administration could shed light on the time course of this inhibitor's efficacy.

Here, we demonstrate direct target engagement of the LDH inhibitor GNE140 in breast and lung cancer. The image data presented demonstrate the ability of hyperpolarized MRSI to visualize the effects of LDH inhibition non-invasively and in real time. The data also demonstrate the high efficacy of GNE140 to inhibit LDH activity, which yields a sizeable reduction in lactate signal in models of breast and lung cancer within 30 minutes. This reduction of LDH activity might be expected to increase flux of pyruvate through pyruvate dehydrogenase, which produces polarized bicarbonate. However, in these measurements at 9.4T there was no discernable bicarbonate signal either before or after inhibition of LDH. Small signals from alanine were also unchanged.

In contrast to GNE140, which inhibits both isoforms of LDH, in models of lung cancer where *LDH-A* is genetically ablated, no appreciable reduction in lactate was observed. IHC analysis of LDH-A protein expression showed that loss of *LDH-A* upon Cre-induction was detectable but incomplete. This result is similar to what was described earlier[10], possibly due to incomplete bioavailability of tamoxifen in perfused regions of the tumors, or due to a survival advantage of tumor cells without *LDH-A* extinction. Regardless of the mechanism that led to incomplete LDH-A protein extinction in the conditional knock-out model, it is noteworthy that a reduced level of LDH-A protein did not correspond to an appreciable reduction in lactate signal. It is therefore hypothesized either that a reduced expression of LDH-A protein is sufficient to mediate pyruvate/lactate label exchange, or that the LDH-B isoenzyme is sufficient to mediate this exchange, despite its lower affinity for pyruvate, and that the tumors were able to mobilize one or both of these compensatory mechanisms within 7 days of Cre-mediated loss of *LDH-A*. A further possibility is that altered MCT expression following *LDH-A* ablation may alter the transport of pyruvate and lactate in a way that compensates for the reduction in LDH-A protein levels. IHC analysis of MCT1 and MCT4 shows low levels of expression in tumors following *LDH-A* ablation compared to neighboring muscle, and no dramatic differences are seen between animals that have undergone *LDH-A* ablation and animals with intact *LDH-A*. One further intriguing possibility is that the potentially large blood volume in the lungs partially accounts for this result. This is because erythrocytes, which rely exclusively on glycolysis and express only LDH-B, have the potential to convert pyruvate to lactate and are unaffected by *LDH-A* deletion. In the analysis presented above, large vessels (which are readily identified by their large intravascular pyruvate signal) were excluded from the regions of interest that were used for computation of the lactate-to-pyruvate ratios. CT perfusion measurements in human lung tumors have reported a blood volume of roughly 6%, a value consistent across different tumor types[25]. Based on this, at a typical hematocrit, erythrocytes occupy on the order of 3% of the total tumor volume. Given the relatively small volume occupancy of the erythrocytes, it appears unlikely that their metabolism dominates the pyruvate/lactate exchange in solid tumors even if their rates of glycolysis are high. Nevertheless the erythrocytes will produce a 'baseline' signal that is independent of *LDH-A* status and their contribution is an important caveat in the interpretation of the results. Our data show that near complete extinction of LDH activity can be achieved with the medicinal inhibitor.

The results from this work support the use of hyperpolarized ^{13}C MR for *in vivo*, non-invasive monitoring of the metabolic effects of inhibition of LDH, and more widely in studies relating to modifications to the Warburg effect. The biomarker of metabolism took the form of the lactate-to-pyruvate ratio, which provides a surrogate measure relating to cancer aggressiveness and progression[26,27], and showed a significant reduction in cases of LDH inhibition by the drug GNE140 but remained relatively consistent in the EGFR-driven lung cancer model following genetic ablation of *LDH-A*. Use of hyperpolarized ^{13}C MR and the lactate-to-pyruvate ratio in oncological studies allows interrogation of the metabolic pathways associated with the Warburg effect and aerobic glycolysis that are prominent in cancer cells. This may be particularly pertinent in future drug development and trials, particularly with increasing demonstration of hyperpolarized ^{13}C MRI translated to human studies[28].

Acknowledgements

Abbreviations

DNP	dynamic nuclear polarization
EGFR	epidermal growth factor receptor
EPSI	echo-planar spectroscopic imaging
HIF1α	hypoxia-inducible factor 1α
IHC	immunohistochemical
LDH	lactate dehydrogenase
MCT	monocarboxylate transporter
MRSI	magnetic resonance spectroscopic imaging
NSCLC	non-small cell lung cancer
ROIs	regions of interest
TNBC	triple-negative breast cancer

References

1. Warburg O. On respiratory impairment in cancer cells. Science (80-). 1956;124(3215):269–270.

2. Le A, Cooper CR, Gouw AM, et al. Inhibition of lactate dehydrogenase A induces oxidative stress and inhibits tumor progression. Proc Natl Acad Sci. 2010;107(5):2037–2042. doi:10.1073/pnas.0914433107 [PubMed: 20133848]

3. Rodic S, Vincent MD. Reactive oxygen species (ROS) are a key determinant of cancer's metabolic phenotype. Int J Cancer. 2018;142:440–448. doi:10.1002/ijc.31069 [PubMed: 28940517]

4. Gatenby RA, Gillies RJ. Why do cancers have high aerobic glycolysis? Nat Rev Cancer. 2004;4:891–899. doi:10.1038/nrc1478 [PubMed: 15516961]

5. Husain Z, Seth P, Sukhatme VP. Tumor-derived lactate and myeloid-derived suppressor cells Linking metabolism to cancer immunology. Oncoimmunology. 2013;2(11):e26383.

6. Romero-Garcia S, Moreno-Altamirano MMB, Prado-Garcia H, Sánchez-García FJ. Lactate Contribution to the Tumor Microenvironment: Mechanisms, effects on immune Cells and Therapeutic Relevance. Front Immunol. 2016;7:52. doi:10.3389/fimmu.2016.00052 [PubMed: 26909082]

7. Vander Heiden MG, Cantley LC, Thompson CB. Understanding the Warburg effect: The metabolic requirements of cell proliferation. Science (80-). 2009;324(5930):1029–1033.

8. Sullivan MR, Vander Heiden MG. Determinants of nutrient limitations in cancer. Crit Rev Biochem Mol Biol. 2019;1–15. doi:10.1080/10409238.2019.1611733 [PubMed: 30691308]

9. Kato Y, Ozawa S, Miyamoto C, Maehata Y, Suzuki A, Maeda T. Acidic extracellular microenvironment and cancer. Cancer Cell Int. 2013;13(1):89. [PubMed: 24004445]

10. Xie H, Hanai JI, Ren JG, et al. Targeting lactate dehydrogenase-A inhibits tumorigenesis and tumor progression in mouse models of lung cancer and impacts tumor-initiating cells. Cell Metab. 2014;19(5):795–809. doi:10.1016/j.cmet.2014.03.003 [PubMed: 24726384]

11. Seth P, Grant A, Tang J, et al. On-target Inhibition of Tumor Fermentative Glycolysis as Visualized by Hyperpolarized Pyruvate. Neoplasia. 2011;13(1):60–71. doi:10.1593/neo.101020 [PubMed: 21245941]

12. Day SE, Kettunen MI, Gallagher FA, et al. Detecting tumor response to treatment using hyperpolarized 13C magnetic resonance imaging and spectroscopy. Nat Med. 2007;13(11):1382–1387. doi:10.1038/nm1650 [PubMed: 17965722]

13. Witney TH, Kettunen MI, Brindle KM. Kinetic modeling of hyperpolarized 13C label exchange between pyruvate and lactate in tumor cells. J Biol Chem. 2011;286(28):24572–24580. doi:10.1074/jbc.M111.237727

14. Hu H, Juvekar A, Lyssiotis CA, et al. Phosphoinositide 3-Kinase regulates Glycolysis through mobilization of Aldolase from the Actin cytoskeleton. Cell. 2016;164(3):433–446. doi:10.1016/j.cell.2015.12.042 [PubMed: 26824656]

15. Park I, Bok R, Ozawa T, et al. Detection of early response to Temozolomide treatment in brain tumors using hyperpolarized 13C MR metabolic imaging. J Magn Reson Imaging. 2011;33(6):1284–1290. doi:10.1002/jmri.22563 [PubMed: 21590996]

16. Ward CS, Venkatesh HS, Chaumeil MM, et al. Noninvasive detection of target modulation following Phosphatidylinositol 3-Kinase inhibition using hyperpolarized 13C magnetic resonance spectroscopy. Cancer Res. 2010;70(4):1296–1305. doi:10.1158/0008-5472.CAN-09-2251 [PubMed: 20145128]

17. Dutta P, Le A, Vander Jagt DL, et al. Evaluation of LDH-A and Glutaminase Inhibition In Vivo by Hyperpolarized 13 C-Pyruvate Magnetic Resonance Spectroscopy of Tumors. Cancer Res. 2013;73(14):4190–4196. doi:10.1158/0008-5472.CAN-13-0465 [PubMed: 23722553]

18. Boudreau A, Purkey HE, Hitz A, et al. Metabolic plasticity underpins innate and acquired resistance to LDHA inhibition. Nat Chem Biol. 2016;12(10):779–786. doi:10.1038/nchembio.2143 [PubMed: 27479743]

19. Zdralevic M, Brand A, Di Ianni L, et al. Double genetic disruption of lactate dehydrogenases A and B is required to ablate the " Warburg effect " restricting tumor growth to oxidative metabolism. J Biol Chem. 2018;293(41):15947–15961. doi:10.1074/jbc.RA118.004180

20. Liu X, Holstege H, van der Gulden H, et al. Somatic loss of BRCA1 and p53 in mice induces mammary tumors with features of human BRCA1-mutated basal-like breast cancer. Proc Natl Acad Sci. 2007;104(29):12111–12116.

21. Juvekar A, Burga LN, Hu H, et al. Combining a PI3K inhibitor with a PARP inhibitor provides an effective therapy for BRCA1-related breast cancer. Cancer Discov. 2012;2(11):1048–1063. doi:10.1158/2159-8290.CD-11-0336 [PubMed: 22915751]

22. Regales L, Balak MN, Gong Y, et al. Development of new mouse lung tumor models expressing EGFR T790M mutants associated with clinical resistance to kinase inhibitors. PLoS One. 2007;2(8):e810. doi:10.1371/journal.pone.0000810 [PubMed: 17726540]

23. Hill DK, Orton MR, Mariotti E, et al. Model Free Approach to Kinetic Analysis of Real-Time Hyperpolarized 13C Magnetic Resonance Spectroscopy Data. PLoS One. 2013;8(9):e71996. doi:10.1371/journal.pone.0071996

24. Juvekar A, Hu H, Yadegarynia S, et al. Phosphoinositide 3-kinase inhibitors induce DNA damage through nucleoside depletion. Proc Natl Acad Sci. 2016;113(30):E4338-E4347. doi:10.1073/pnas.1522223113

25. Spira D, Neumeister H, Spira SM, et al. Assessment of Tumor Vascularity in Lung Cancer Using Volume Perfusion CT (VPCT) With Histopathologic Comparison : A Further Step Toward an Individualized Tumor Characterization. J Comput Assist Tomogr. 2013;37(1):15–21. [PubMed: 23321828]

26. Chen HY, Gordon JW, Bok RA, et al. Pulse sequence considerations for quantification of pyruvate-to-lactate conversion kPL in hyperpolarized 13C imaging. NMR Biomed. 2019;(32):e4052. doi:10.1002/nbm.4052
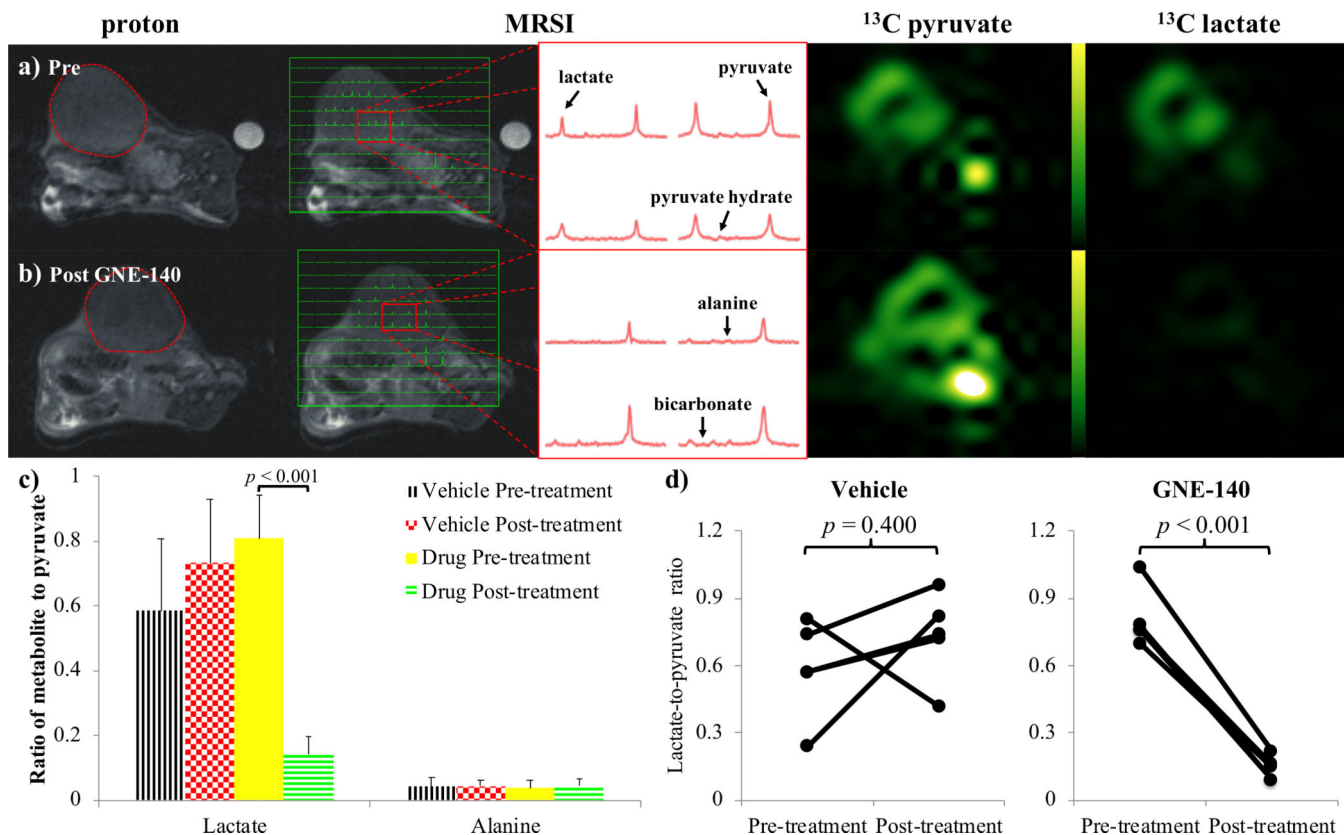
27. Daniels CJ, Mclean MA, Schulte RF, et al. A comparison of quantitative methods for clinical imaging with hyperpolarized. 2016;(June 2015):387–399. doi:10.1002/nbm.3468

28. Kurhanewicz J, Vigneron DB, Brindle K, et al. Clinical Translation in Oncology. Neoplasia. 2019;21(1):1–16. doi:10.1016/j.neo.2018.09.006 [PubMed: 30472500]
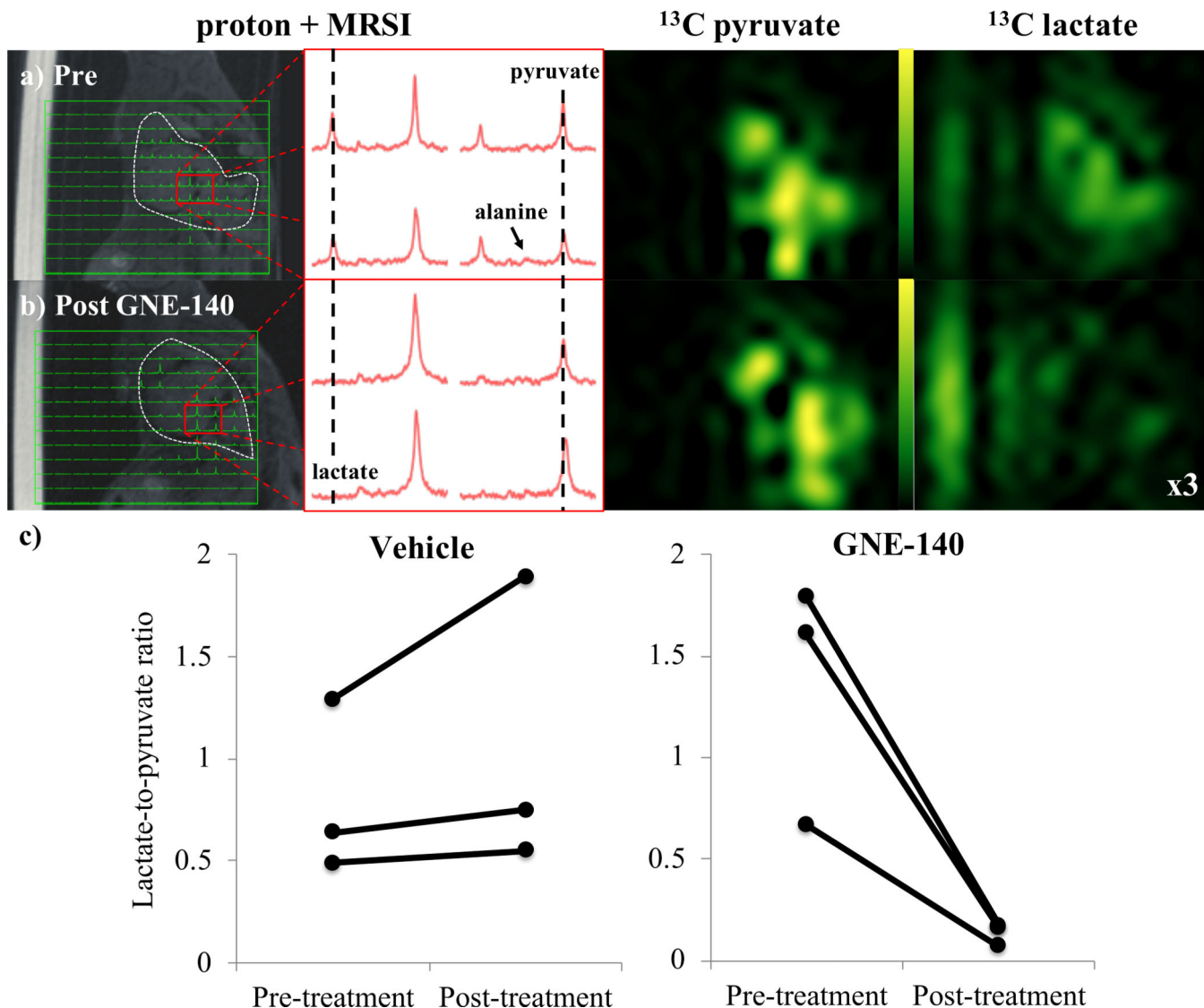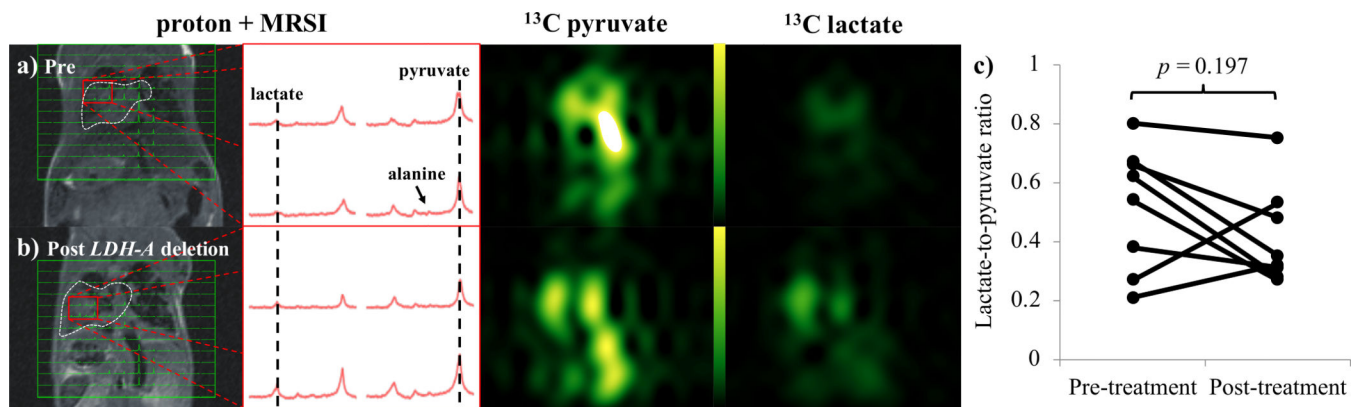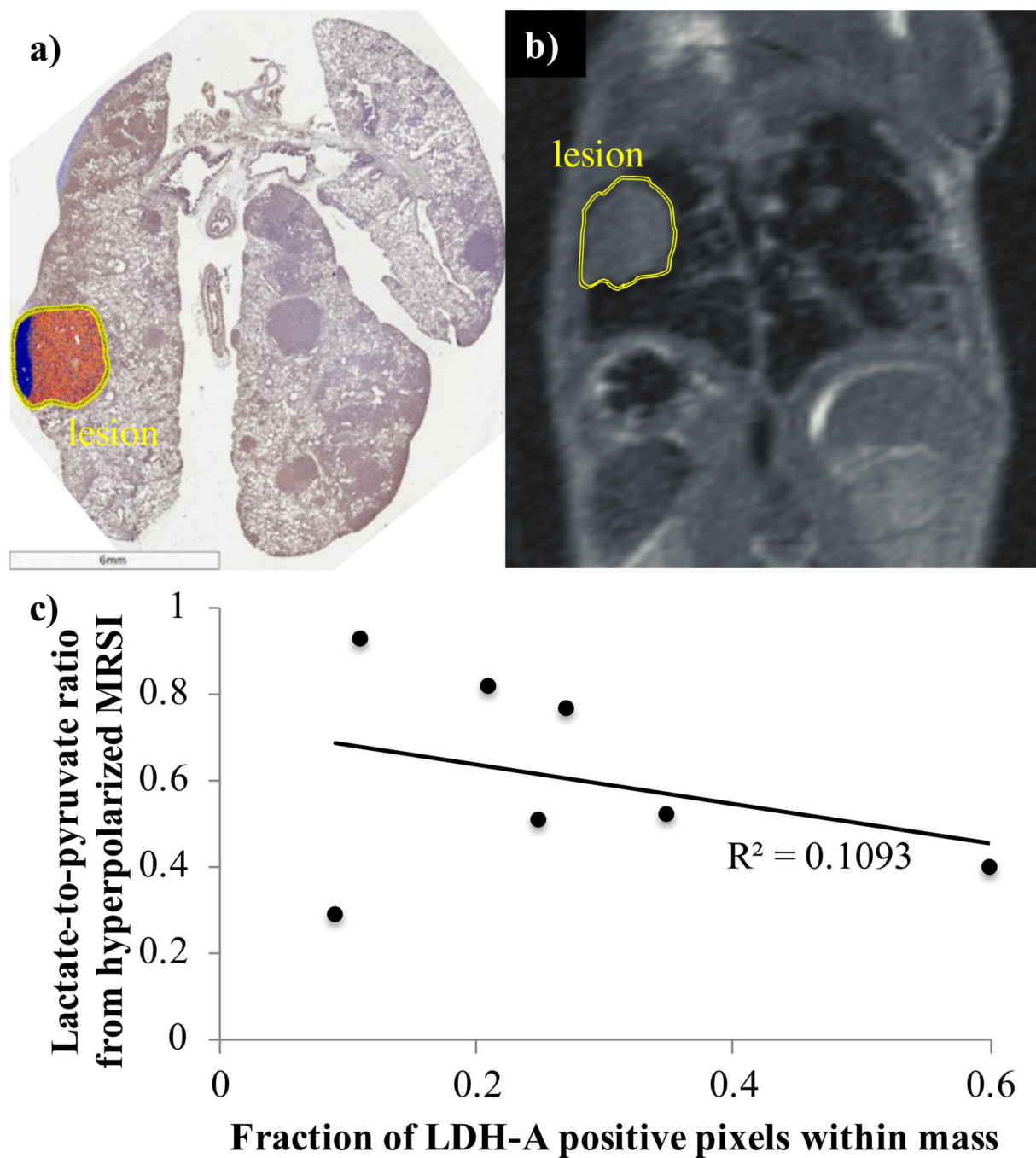
Figure 1.
Images acquired in a model of triple-negative BRCA1-related breast cancer, a) before, and b) after administration of GNE140. From the left: proton; ^{13}C MRSI voxels overlaid onto proton; representative ^{13}C spectra from the tumor; pyruvate; and lactate, images. Pyruvate and lactate images from the same ^{13}C MRSI acquisition are displayed on the same scale. The expected location of the bicarbonate signal (aliased due to the spectral width of the MRSI acquisition) is indicated in the lower right spectrum of the bottom center panel. c) Column plot of the ratio of lactate and alanine peaks to pyruvate peaks integrated over the ^{13}C MRSI data acquisition. Values and error bars represent the mean and standard deviation calculated over the breast cancer model mice in each group (i.e. n=5) respectively. Brackets highlight p-values from paired two-tailed Student's t-tests of the results pre- and post- treatment with the drug GNE140 and DMSO or the vehicle DMSO only. d) Scatter plots showing the lactate-to-pyruvate ratios in the breast cancer model before and after administration of vehicle (left) and GNE140 (right).

Figure 2.
Images acquired in a model of lung cancer, a) before, and b) after administration of GNE140. From the left: ^{13}C MRSI voxels overlaid onto proton; representative ^{13}C spectra from the tumor; pyruvate; and lactate, images. A vial of acetate used for reference (located approximately 50Hz from lactate in ^{13}C spectra) appears in proton and lactate images to the left of the mouse. The signal intensity in the lactate image from ^{13}C MRSI post administration of the LDH inhibitor is multiplied by 3 (relative to signal in the pyruvate image) to highlight the absence of lactate signal. c) Scatter plots show the change in lactate-to-pyruvate ratios from hyperpolarized ^{13}C MRSI in the EFGR-driven lung cancer tumors before and after administration of vehicle (left) and GNE140 (right). N=3 for both control and treated groups.
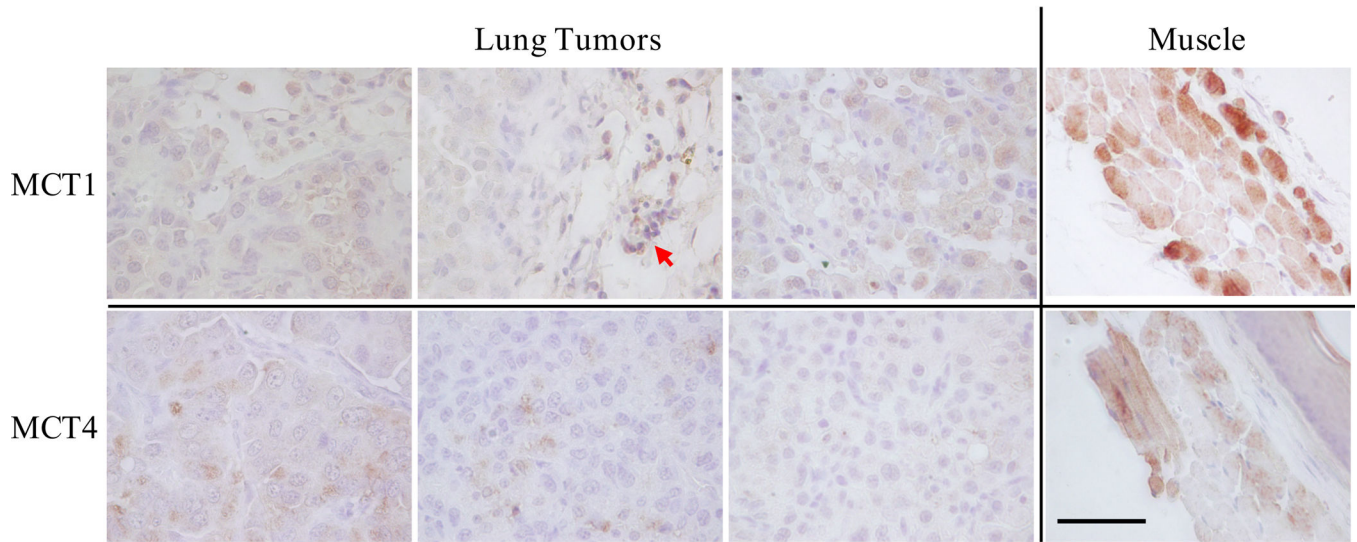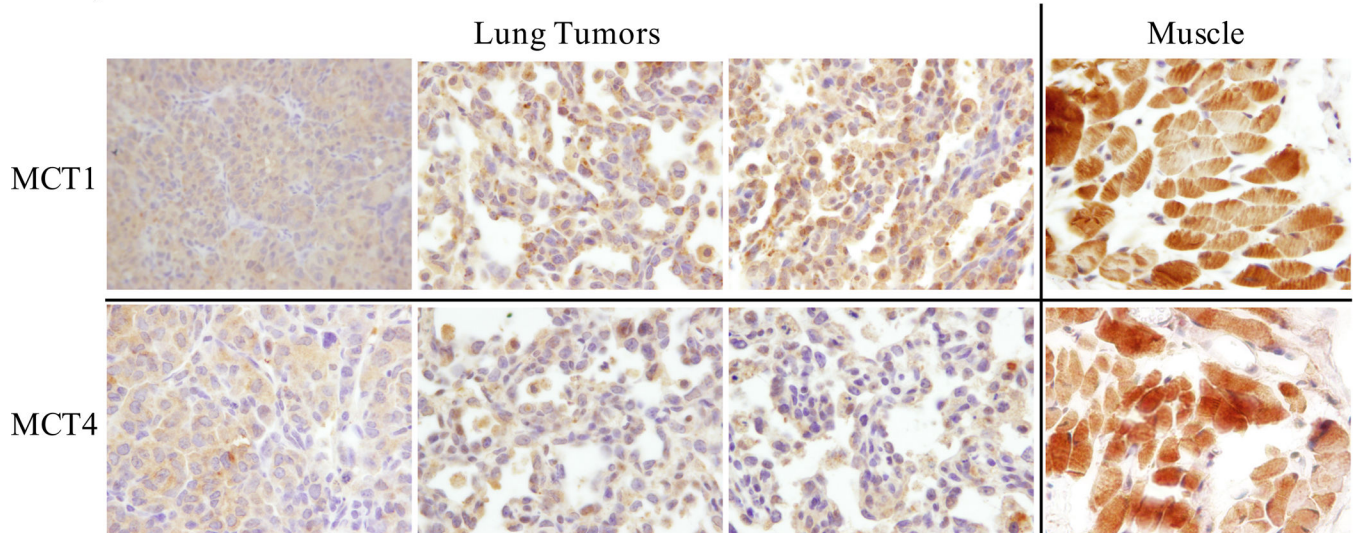
Figure 3.
Images acquired in a model of lung cancer, a) before, and b) after administration of tamoxifen to initiate *LDH-A* deletion. From the left: ^{13}C MRSI voxels overlaid onto proton; representative ^{13}C spectra from the tumor; pyruvate; and lactate, images. Pyruvate and lactate images from the same ^{13}C MRSI acquisition are displayed on the same scale. c) Scatter plot shows the change in lactate-to-pyruvate ratios from hyperpolarized ^{13}C MRSI in the lung cancer model before and after administration of tamoxifen to initiate *LDH-A* deletion.

Figure 4.
Images from a) IHC staining for LDH in a sample of lung tissue, and b) the matching proton MRI, showing correspondence between the tissue sample and imaging. c) Scatter plot showing the lactate-to-pyruvate ratios from hyperpolarized ^{13}C MRSI against the percentage of LDH-A positive pixels from corresponding samples of lung masses.

a) Post Tamoxifen Treatment:

b) Untreated:

Figure 5.
IHC staining for the transporters MCT1 and MCT4 in three representative animals, a) following tamoxifen administration to induce deletion of *LDH-A*, and b) untreated animals. Tumors from the three mice shown in the upper panel are the same that contribute to data plot in Figure 4c. Robust staining of the musculature (rightmost panels) as well as mono-nuclear cells (red arrow) served as an internal control for the staining. Consistent with prior reporting, expression of the transporters was low. Slides were processed according to standard protocol for IHC with antibodies against MCT1 and MCT4. Scale bar = 100 μm.